Engineering Geology 184 (2015) 96–103

Contents lists available at ScienceDirect

Engineering Geology

journal homepage: www.elsevier.com/locate/enggeo

Slope stability analysis under unsaturated conditions: Case studies of rainfall-induced failure of cut slopes

Seboong Oh [a,*], Ning Lu [b]

[a] Department of Civil Engineering, Yeungnam University, Gyeongsan, Republic of Korea
[b] Department of Civil and Environmental Engineering, Colorado School of Mines, Golden, CO 80401, United States

ARTICLE INFO

Article history:
Received 18 July 2014
Received in revised form 11 October 2014
Accepted 10 November 2014
Available online 17 November 2014

Keywords:
Slope stability
Effective stress
Shear strength
Suction stress
Unsaturated soil
Finite elements

ABSTRACT

We present two case studies of rainfall-induced failure of engineered slopes. The traditional limit equilibrium and finite element methods are expanded to unsaturated conditions using a generalized effective stress framework. Because effective stress is represented by the suction stress characteristic curve (SSCC), and the SSCC and the soil water retention curve (SWRC) have been unified with the same set of hydromechanical parameters, the expanded framework requires only three hydromechanical parameters in addition to those used for saturated slope stability analysis. Using recorded rainfall, measured shear strength parameters and the SWRC, and site geology, transient slope stability analyses are conducted to reconstruct the failure events. We find that, despite differences in slope geometry, hydromechanical properties, shear strength, and rainfall history, the actual failure occurred when the simulated factor of safety approaches its minimum below 1.0. It is shown that the hydromechanical framework under the suction stress-based effective stress can reconcile the observed timing of failure.

1. Introduction

Limit equilibrium (LE) methods are the most widely used for analyzing slope stability and designing engineered slopes. The simplicity and versatility of the LE methodology rest with the concept that the geometry of the potential failure surface in a slope is known a-priori and the slope can be discretized into finite vertical slices. Each slice is then analyzed using principles of force and/or moment equilibrium (e.g., Peterson, 1955; Duncan and Wright, 2005) for its contribution to the stability of the slope. Over the previous century, a variety of LE techniques have been developed to determine stability conditions, depending on the equations of equilibrium that are included and what assumptions are made to account for inter-slice forces (e.g., Bishop, 1954; Morgenstern and Price, 1965; Spencer, 1967; Duncan, 1996). In recent years, to accurately compute inter-slice forces and seepage conditions, advanced quantitative methods such as analytical, finite elements and finite differences have been developed and incorporated with LE algorithms (e.g., Ugai and Leshchinsky, 1995; Duncan, 1996; Dawson et al., 1999).

The key indicator in slope stability analysis is the factor of safety (FOS), which is commonly defined as the ratio of the resisting shear force to the driving shear force along a failure surface. To better calculate the factor of safety and identify the failure surface, recent advances have been made using either the "gravity increase method", or the "strength reduction method" (e.g., Dawson et al., 1999; Griffiths and Lane, 1999; Krahn, 2003), or the field of local factor of safety method (Lu et al., 2012).

One common assumption made in most of the existing slope stability methods is that along the failure surface pore water pressure is positive or zero (e.g., Bishop, 1954; Morgenstern and Price, 1965; Duncan, 1996). In reality, under rainfall conditions, the degree of saturation within a slope and along a failure surface could be highly variable and pore water pressure could be negative (e.g., Godt et al., 2009; Borja and White, 2010; Buscarnera and Whittle, 2012). Thus this assumption could lead to incorrect treatment of effective stress or shear strength, and ultimately, inaccuracy in computing the factor of safety of a slope. Although some recent studies are specifically focused on infiltration induced landslides, most of them combine analysis of the hydrological behavior with an infinite or analytical slope-stability analysis or examine rainfall patterns and relate them to slope stability over large areas that include multiple landslides (e.g., Iverson, 2000; Crosta and Frattini, 2003). However, most of these studies only consider slope failure below the groundwater table, overlooking the contribution of effective stress (suction stress) to the strength of the soil under transient unsaturated flow conditions.

In recent years, slope-stability analyses have been expanded to include coupled hydromechanical processes under variably saturated conditions (e.g., Griffiths and Lu, 2005; Lu and Godt, 2008; Borja and White, 2010; Buscarnera and Whittle, 2012; Lu et al., 2013). These analyses incorporate the variation of saturation, leading to more

* Corresponding author.
E-mail addresses: sebungoh@yu.ac.kr (S. Oh), ninglu@mines.edu (N. Lu).

http://dx.doi.org/10.1016/j.enggeo.2014.11.007
0013-7952/

accurate assessments of stability of slopes under infiltration conditions and demonstrate that a better physical representation of water flow and stress can be attained in unsaturated soils. When water infiltrates into hillslopes, the water content of the hillslope materials and the water table level vary accordingly. Changes in the water content of the soil imply changes in weight, matric suction, effective stress, and stability of a slope. Thus, understanding the physical conditions (i.e., if they are saturated or not) within variably saturated slopes when failures occur is needed for accurate assessment and prediction. The study presented here presents some of the first documented case studies of failed engineered cut slopes analyzed by employing unsaturated soil mechanics concept. The main objectives of this work are as follows: (1) to quantitatively understand why slopes failed at the studied sites under rainfall conditions, and (2) to use these case studies to demonstrate that the failure of unsaturated engineered cut slopes under transient rainfall conditions can be reconciled using the hydromechanical framework described below.

2. An LE/FE framework for variably saturated slope stability analysis

In comparison with the classical LE and finite element-based slope stability analysis, the framework employed in this work involves two major enhancements: (1) accounting for transient unsaturated flow, and (2) implementing a unified effective stress for all degrees of saturations. The framework involves a one-way hydromechanical coupling in which simulated transient water content and matric suction fields are used to compute fields of total and effective stress, and consequently, the factor of safety. For completeness, the essentials of such framework are briefly described below.

Transient fields of water content and pressure head in variably saturated soil slopes are governed by Richards' equation (Richards, 1931):

$$\nabla \cdot k(h)\nabla H = \frac{\partial \theta(h)}{\partial t} \tag{1}$$

where h is the pressure head or suction head; H is the total head being the sum of suction head and elevation; $k(h)$ is the hydraulic conductivity function (HCF); and $\theta(h)$ is the pressure-head dependent volumetric water content (or water content hereafter). The relation between the pressure head and water content is called the soil water retention curve (SWRC). To solve Eq. (1) for fields of suction head and water content, two characteristic functions, namely, SWRC and HCF, have to be defined and known. There are many models for the SWRC and HCF, and here we adopt the widely used van Genuchten's (1980) model for the SWRC and van Genuchten–Mualem's model for the HCF (Mualem, 1976; van Genuchten, 1980) with respect to matric suction ($u_a - u_w$), i.e.:

$$\frac{\theta - \theta_r}{\theta_s - \theta_r} = \left[\frac{1}{1 + \{\alpha(u_a - u_w)\}^n}\right]^{1-1/n} \tag{2}$$

$$k = k_s \frac{\left[1 - \{\alpha(u_a - u_w)\}^{n-1}\left[1 + \{\alpha(u_a - u_w)\}^n\right]^{1/n-1}\right]^2}{\left[1 + \{\alpha(u_a - u_w)\}^n\right]^{1/2-n/2}} \tag{3}$$

where u_a is the pore air pressure and u_w is the pore water pressure, θ_r and θ_s are the volumetric water contents at the residual and saturated states, respectively, α is a parameter that represents the inverse of the air entry suction, n is the pore size parameter, and k_s is the saturated hydraulic conductivity. With appropriate initial conditions, boundary conditions (such as infiltration rate at the slope surface), and soil parameters, Eqs. (1)–(3) can be solved to obtain fields of suction head and water content in slopes under variably saturated conditions (e.g., Lu and Godt, 2008; Borja and White, 2010; Godt et al., 2012).

Once fields of water content and matric suction are obtained, the total stress and effective stress fields can be obtained. The total stress fields are governed by the following linear momentum equilibrium equation:

$$\nabla \cdot \boldsymbol{\sigma} + \frac{\gamma}{g}\mathbf{b} = 0 \tag{4}$$

where, $\boldsymbol{\sigma}$ is stress tensor with 3 independent total stress variables in two-dimensional space; $\mathbf{b}$ is vector of body forces with 2 components; γ is the unit weight of materials and depends on water content; g is acceleration due to gravity. The effective stress field is computed by the suction stress-based equation (Lu and Likos, 2004, 2006):

$$\sigma' = \sigma - u_a - \sigma^s \tag{5}$$

where the suction stress characteristic curve σ^s (or SSCC) can be expressed as a function of matric suction ($u_a - u_w$) (Lu and Likos, 2004; Lu et al., 2010):

$$\sigma^s = -\frac{\theta - \theta_r}{\theta_s - \theta_r}(u_a - u_w) = -(u_a - u_w)\left[\frac{1}{1 + \{\alpha(u_a - u_w)\}^n}\right]^{1-1/n} \tag{6}$$

where parameters α and n are identical to van Genuchten's (1980) SWRC model (Eq. (2)) and Mualem's (1976) HCF model (Eq. (3)). Note that using a common set of parameters to define a soil's SWRC, HCF, and SSCC minimizes the number of parameters involved in a variably saturated slope stability analysis; the other remaining parameters in the hydromechanical framework are the drained cohesion c' and friction angle ϕ' defined in the Mohr–Coulomb failure criterion. The interrelations among a soil's SWRC, HCF, and SSCC have been theoretically established and experimentally validated (van Genuchten (1980) and Wayllace and Lu (2011) for the relation between SWRC and HCF; Lu and Likos (2006), Lu et al. (2010), Song et al. (2012), and Lu and Kaya (2013) for the relations among SWRC, HCF, and SSCC).

Finally, once the fields of total and effective stresses are obtained, the classical LE analysis with finite element (FE) solutions is used to determine the FOS of the slope under transient infiltration conditions (e.g., Godt et al., 2012). A method of slices is used to compute the FOS along failure surfaces and to search a critical slip surface (a surface with the lowest FOS). The FOS is commonly defined as the ratio of the shear resistance and the mobilized shear force along the entire length of the slip surface as:

$$FOS = \frac{\sum_i \left(\tau_f l_{base}\right)_i}{\sum_i (\tau l_{base})_i} = \frac{\sum_i \left[(c' + \sigma' tan\varphi')\ \ l_{base}\right]_i}{\sum_i (\tau l_{base})_i} \tag{7}$$

where i is the slice index and l_{base} is the base length of each slice, τ_f and τ are respectively the shear strength and shear stress according to FE solutions on the base of slices, c' is the drained cohesion and ϕ' is the drained friction angle. The effective stress shown in Eq. (7) is obtained by using Eqs. (5)–(6) wherein total stress and matric suction are obtained by solving Eqs. (1)–(4). In this work, the failure surfaces were all estimated based on a field investigation of surface exposures and some preliminary slope stability analysis.

3. Site geology and material properties

In the mountainous areas of Korea there are about 1 million existing cut slopes, which, for comparison, is ~20 times more cut slopes as in Hong Kong (Lee and Hencher, 2009). However, adequate design and geotechnical survey are rarely done prior to construction, due to the lack of standard design methodologies for unsaturated conditions and a general reluctance to invest resources in planning. As a result, the assessment of the stability of cut slopes is rarely realistic at the design stage. Consequently, cut slopes in Korea fail frequently, even during construction phases. One of the challenges in the practice of slope analysis is the lack of the laboratory test data necessary to obtain

unsaturated soil properties such as the SWRC and HCF. These tests are often problematic and time-consuming for residual soils. Even though the structure of these soils is consistent with the structure of the parent rock, their wide variability in grain sizes, fracture network, and heterogeneity makes these tests difficult.

The two cut slope failure sites are near Hadong City and Pohang City and their locations are shown in Fig. 1. Cross-sections at the sites obtained from basic geologic and geotechnical survey are shown in Fig. 2 with the finite element meshes. The slip surfaces are determined as the critical surface at the date of failure from the current stability analysis. They are similar to what have been mapped from the field evidence collected at the sites after the failures. The stratum of Cretaceous rocks contains mainly granitic gneiss and weathered granite in Hadong (Figure 2a) and mudstone and shale in Pohang (Figure 2b). Over the geologic history, the rock layer has been exposed at the surface and the layer generally lies in flatly. The rock layer has been weathered heavily below the residual soil layers and contains multiple fractures with joints, bedding planes, and faults. The upper layer of the slopes is characteristically composed of residual soils with a depth from 5 m to 20 m. Such a geological setting described at the two cut slope sites is typical of many slopes in the southeast part of Korean peninsula.

The Hadong slope (Figure 2a) is an engineered cut slope along a road that has been in service without any instability problems for several years following construction. However, in the middle of July in 2009, after heavy rainfall of 1029 mm in three months, the Hadong slope failed with failure patterns shown in Fig. 2a. The excavation and construction of the Pohang slope were completed around the end of October 2010. The Pohang slope failed at the end of June 2011, after a three-month rainfall of 420 mm. Considering that the average annual rainfall in this part of Korea is about 900–1300 mm, the rainfall that lead to the slope failures can be considered heavy at Hadong site but typical at Pohang site. The angle of the cut slopes ranges 40–45° with respect to the horizontal plane. Due to the previous practice of saturated slope design, the cut slopes had been designed to be almost saturated by the water table near surface. However, using unreliable parameters on the saturated shear strength, the slopes were obviously not stable from a traditional slope stability perspective.

Under the hydromechanical framework, the properties needed for slope stability analysis are categorized into four groups: physical, strength, deformation, and hydromechanical as shown in Tables 1 and 2. The first three groups as well as the saturated hydraulic conductivity and porosity are used in the classical slope stability analysis under transient saturated seepage conditions. For slope stability analysis under transient unsaturated seepage conditions using the hydromechanical framework only three additional parameters are needed, namely the residual water content θ_r, the air-entry pressure u_b, and the pore size distribution parameter n. Due to the non-homogeneous nature of residual soils, it is challenging to obtain representative, undisturbed soil samples at these sites for hydromechanical property testing. For instance, during the sampling process, it was found that some of the samples were friable and highly fractured; this is particularly true for samples with large dimensions. In order to obtain representative and consistent results, it was necessary to perform a sufficient number of tests on both undisturbed (when possible) and remolded soil specimens. A number of specimens were remolded by static compaction to replicate in-situ conditions of water content and density. The axis translation technique was used to obtain the soil–water retention data. The SWRCs were obtained from the pressure plate tests and fit to the van Genuchten model using the RETC code (van Genuchten et al., 1991). Direct shear tests were conducted under saturated conditions in order to obtain shear strength parameters of soil. Multistage triaxial tests were conducted under unsaturated conditions in order to confirm the principle of effective stress defined by Eq. (5). The values for these hydromechanical properties defining the SWRC, HCF, and failure envelope are listed in Table 2, and the corresponding SWRC, HCF, and failure envelopes are plotted in Fig. 3.

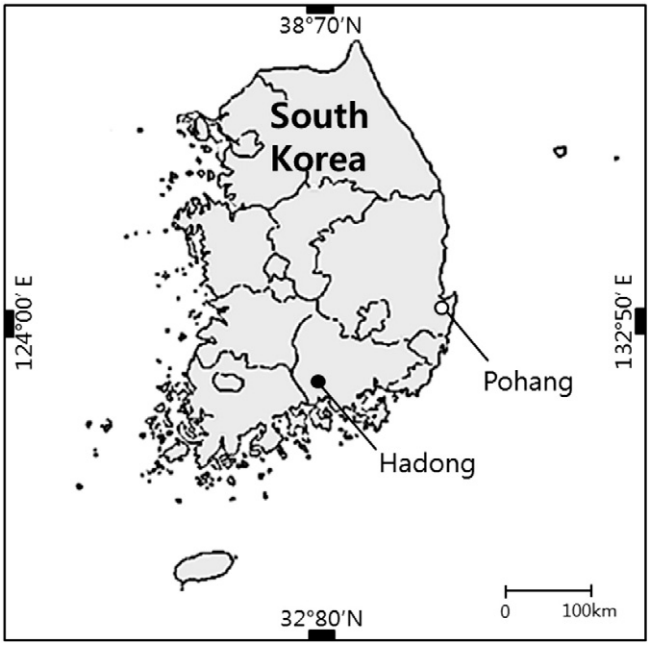

Fig. 1. Locations of the two cut slope failure sites in Korea.

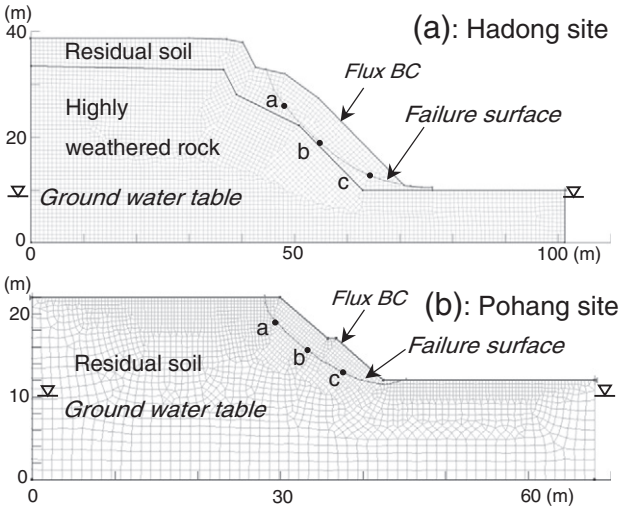

Fig. 2. Geologic layers and finite element meshes of the failure slopes: (a) Hadong site, and (b) Pohang site.

As shown in Fig. 3a and Table 2, the air entry pressures u_b are 22.5 kPa for the Hadong residual soil (SW), and 27.9 kPa for the Pohang residual soil, respectively. For the Hadong residual soil, the pore size distribution parameter n is 1.4, the saturated volumetric water content (porosity) is 0.28, and residual water content is 0.0 (shown in Table 2). The Pohang silty soils are weathered from mudstone and shale, and contain greater than 50% fine-grained materials (Table 1). These soils exhibit some expansive character with an activity value of 0.9 (Table 1). The SWRCs are typical of silty soils: n is equal to 1.1; θ_s is 0.40; and θ_r is 0.12 for the Pohang residual soil. The dry unit weight γ_d obtained for the soil specimens are listed in Table 1. To simplify the computational effort in the transient slope stability analyses, an average bulk unit weight γ_{ave} at 90% saturation were used and are shown in Table 2. Although the bulk unit weight varies under field conditions, it is usually within 10% of its average value. We conducted an additional sensitivity analysis and found that within this range of variation in the unit weight, the change in the minimum FOS is <0.8%.

Table 1
Physical properties of the two cut slope materials.

Samples	USCS	Specific gravity G_s	Particles <75 μm (%)	Void ratio	Dry unit weight γ_d (kN/m^3)	In-situ volumetric water content θ	Plastic limit PL	Plasticity index PI	Activity A
Hadong	SW	2.63	4.7	0.977	13.05	0.081	–	–	–
Pohang	MH	2.65	62.6	0.866	13.93	0.42	36.8	18.3	0.9

Hydraulic conductivity functions were estimated from the SWRCs using a modified Mualem model in order to improve the stability of numerical solutions (Vogel et al., 2001). The resulting curves are shown in Fig. 3b.

In Fig. 3c, the mean effective stress is defined as: $p' = (\sigma_1 + 2\sigma_3)/3 - \sigma^s$, and the deviatoric stress q is defined as: $q = \sigma_1 - \sigma_3$. Direct shear tests were conducted on soil specimens collected from both in order to determine shear strength parameters under saturated conditions, as depicted in Fig. 3c. Under saturated conditions, the drained shear strength parameters c' and ϕ' were experimentally determined and the results are shown in Table 2. The friction angles ϕ' are 34.1° for the Hadong residual soil, and 31.6° for the Pohang residual soil, respectively. The drained cohesion for all soils is zero. To confirm the validity of the effective stress principle by Eq. (5), multi-stage triaxial shear tests for a single sample from each site were performed under unsaturated conditions. Fig. 3c shows the shear strength results from both saturated (direct shear tests) and unsaturated (triaxial test) specimens, in which the unsaturated effective stress (Eq. (5)) is deduced from SSCCs (Eq. (6)) using the SWRC parameters shown in Table 2. As shown, the shear strength of unsaturated soil measured with the triaxial tests is uniquely defined by the saturated or effective shear strength envelops, indicating the validity of the effective stress principle by Eqs. (5)–(6).

The saturated hydraulic conductivity at Hadong site was first determined to be 5.93×10^{-5} m/s using laboratory tests. However, the saturated hydraulic conductivity inferred from the parametric study and constrained by the measured SWRC is about one order of magnitude less (5.6×10^{-6} m/s) than that obtained in the laboratory. This discrepancy is consistent with the assumption that a SW material would have higher saturated hydraulic conductivity value than that of a MH material. Because the parametric study was conducted at the field scale, we chose the smaller value. In the case of Pohang site, the saturated conductivity was also estimated by the similar manner. The parametric study provided a better estimate of saturated hydraulic conductivity relying on inverse numerical modeling of the cross section under two constraints: (1) the applied steady rainfall rate, and (2) the preset FOS value at the time of failure. This approach has been used in the literature to address the field-scale parametric uncertainties in slope stability analysis (e.g., Hoek and Bray, 1981). As shown in Fig. 4, the infiltration rate (intensity) and saturated hydraulic conductivity were varied under a preset FOS value (0.9 for Hadong and 1.0 for Pohang). The saturated hydraulic conductivities at the field scale determined in such manner are shown in Table 2.

Table 2
Geotechnical and hydromechanical properties of the two cut slope materials.

Type	Parameter	Hadong		Pohang
		Soil	Rock	Soil
Strength	c' (kPa)	0	50.0[a]	0
	ϕ' (°)	34.1	35.5[a]	31.6
	γ_{ave} (kN/m^3)	17.41	21.0[a]	18.03
Deformation[b]	E (kPa)	2×10^6		2×10^6
	ν	0.333		0.333
Hydromechanical	k_s (m/s)	5.60×10^{-6c}	1.87×10^{-6c}	3.46×10^{-6c}
	θ_s	0.282		0.398
	θ_r	0		0.12
	u_b (kPa)	22.48		27.93
	n	1.37		1.10

[a] Used values from the site engineering design report (Park, 2013).
[b] Assumed values.
[c] Used values from parametric analysis.

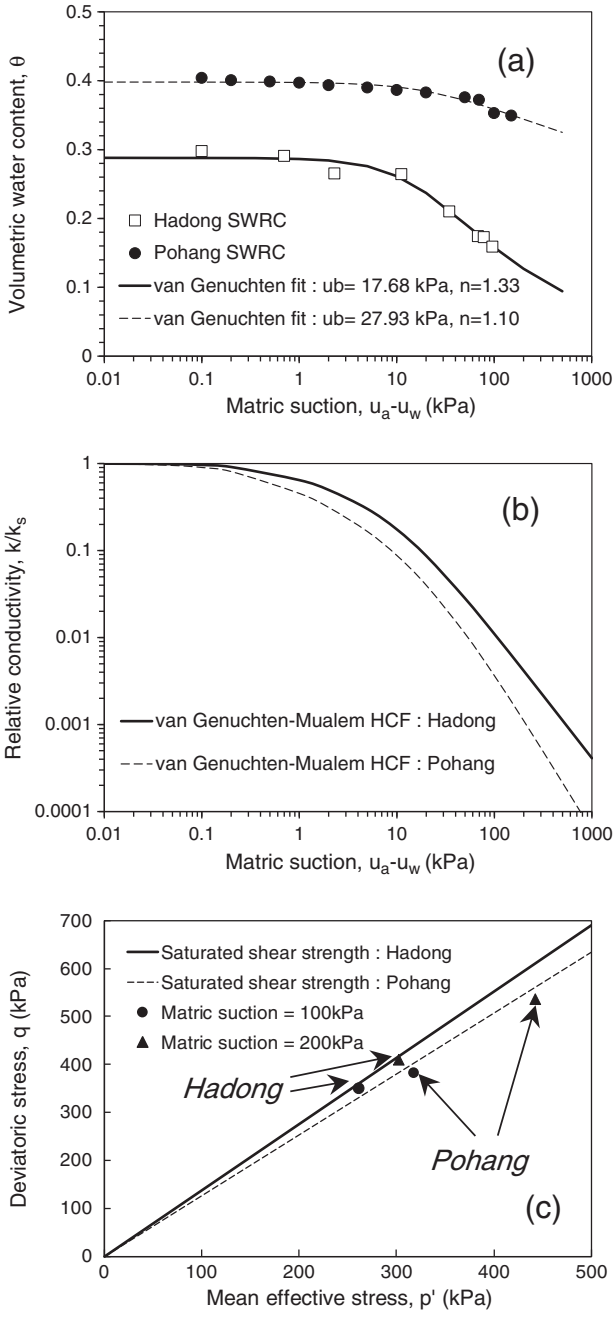

Fig. 3. Hydromechanical and geotechnical properties of: (a) soil water retention data, (b) simulated hydraulic conductivity functions, and (3) shear strength data (saturated and unsaturated) for the slope failure sites.

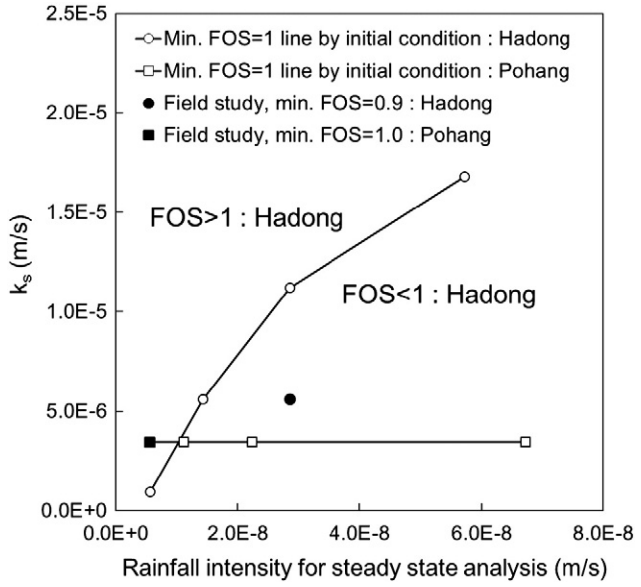

Fig. 4. Results of parametric analysis of field-scale saturated hydraulic conductivity as a function of rainfall intensity under the limit equilibrium state or FOS = 1.0 conditions.

4. Numerical implementation and initial and boundary conditions

The procedures of the LE analysis using a finite element method include three iterative steps: (1) computing transient variably saturated flow fields (pressure head and water content), (2) computing fields of total stress and suction stress (effective stress), and (3) computing the factor of safety along the pre-determined failure surface. The analysis was performed for a single slip surface as part of the failure back analysis. All these procedures are conducted using three modules of Geostudio 2007 (Geo-slope, 2007): SEEP/W to analyze the hydrological behavior due to infiltration (Eq. (1)), SIGMA/W to calculate total stress distribution in the slope layer (Eq. (4)), and SLOPE/W to calculate the factor of safety (Eqs. (5)–(7)). The suction stress (Eq. (6)) and the effective stress (Eq. (5)) are incorporated into the shear strength in the SLOPE/W module as follows:

$$\tau_f = c' + \sigma' \tan\varphi' = c' + \left\{(\sigma - u_a) + \frac{\theta - \theta_r}{\theta_s - \theta_r}(u_a - u_w)\right\}\tan\varphi'. \quad (8)$$

The equation is the same as the failure criterion by Vanapalli et al. (1996), in which the suction stress may be considered as a cohesion, $c = c' - \sigma_s \tan\varphi'$. However, the effective stress theory can generalize suction dependent cohesion by the unique shear strength in variably saturated soils (Figure 3c). The suction stress or the change of effective stress can assess the effect of the hydrological behavior to slope stability due to rainfall as described later.

The variably saturated flow model was established using both steady state and transient analyses with a flux boundary condition to simulate rainfall. The measured SWRC and HCF from the soil samples were used to calculate hydraulic head or pore water pressure in the residual soil layer during infiltration. In the rock layers, the SWRC is assumed to be the same as that of the residual soil. This choice was made due to the lack of testing data and likely has little influence on results given the fact that the failure surfaces are within the residual soil layers and far away from the rock–soil contact. Following the sensitivity analysis to assess the effects of mesh refinement, appropriate mesh configurations were determined for these sites as shown in Fig. 2. For the initial hydrologic conditions, because there was no field measurement of water content or pore pressure, we applied a steady state infiltration rate equal to the antecedent precipitation to the model domain. In the case of Hadong site, the average annual precipitation was used. And in the case of Pohang, the average monthly precipitation was used because there was little antecedent precipitation in the month before the start of the transient analysis. In the literature, many other approaches to assume initial conditions are documented, including hydrostatic and transient infiltration using the recoded precipitation data. Because infiltrating water at the studied sites passes through the predicted failure surface in less than a week and our transient simulation time is greater than 3 months prior to the slope failures, effects of previously mentioned differences resulting from the choice of initial conditions are minimized. For the transient infiltration analysis, a flux boundary condition is applied at the ground surface where the flux corresponds to the recorded rainfall. A zero flux condition is imposed at the bottom of the domain (bedrock). The left and right boundaries consist of a constant head boundary below the water table and a zero flux (horizontal) boundary above the water table. These lateral boundaries are set far away from the slopes. Sensitive study on the effect of the water table location on the stability analysis is conducted where the water table at the left side of the boundary is 5 m above the current position. The result indicates that the water table location has little effect on the results of the slop stability analysis. The initial water table positions shown in Fig. 2 established considering results of the exposure of the water table at the site during slope construction.

Total stress distributions were computed based on the cross-section geometries shown in Fig. 2 and calculated once under body forces using the linear elasticity model implemented in GeoStudio 2007 (Geo-slope, 2007). Young's moduli and Poisson's ratios were assumed from the values within the range for rocks (e.g., Duncan and Wright, 2005) as shown in Table 2. Using the same mesh shown in Fig. 2, the displacement was constrained in the horizontal direction on the left and right side and in the vertical direction on the bottom of the simulation domains. From finite element analyses of unsaturated flow and total stress, effective stress, and the corresponding shear strength and the FOS of the slopes can be calculated at each point along the potential failure surfaces.

5. Reconstruction and analysis of failure events at the sites

5.1. Hadong site

To establish initial conditions, steady state unsaturated flow was first simulated by imposing an annual rainfall of 902 mm (or flow rate of 2.86×10^{-8} m/s) for 2008. Fig. 5 shows the simulation results of the distributions of pore water pressure due to rainfall. At the beginning of the rainfall record shown in Fig. 5a (April 15, 2009), pore water pressure in the residual soil layer (see Fig. 2a for its configuration) gradually decreases from 0 kPa at the water table to −90 kPa above and away from the water table. Note that at this time, the potential failure surface is entirely above the water table.

The transient infiltration following the heavy rainfall episode of 1029 mm shown in Fig. 6a was simulated for the three months prior to July 16, 2009, the date the slope failure occurred. The resulting distribution of pore water pressure is shown in Fig. 5b. At this time, the water table (where pore water pressure is zero) has risen significantly in the region near the toe of the slope. Some of the failure surface (dashed line) is saturated and shows positive pore water pressure in Fig. 5b, but larger portion of the failure surface is unsaturated with negative pore water pressure as low as ~−10 kPa.

The layer in the vicinity of the slope face was fully saturated due to rainfall and pore water pressure increased to almost zero. On the failure surface, values of suction stress are similar to that of pore water pressure, since the degree of saturation is about 1.0 on July 16, as shown in Fig. 6a. According to the effective stress principle defined by Eq. (5), changes in effective stress are the changes in suction stress. Therefore, at this site, effective stress has reduced significantly during this heavy rainfall episode.

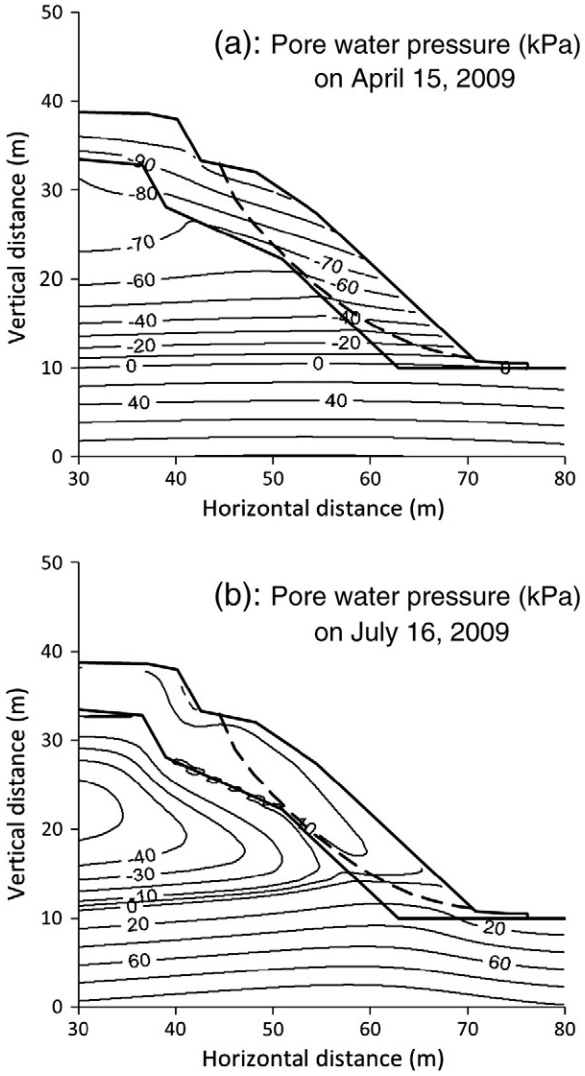

Fig. 5. Simulated results at Hadong site: (a) pore water pressure (kPa) on April 15, 2009, and (b) pore water pressure (kPa) on July 16, 2009.

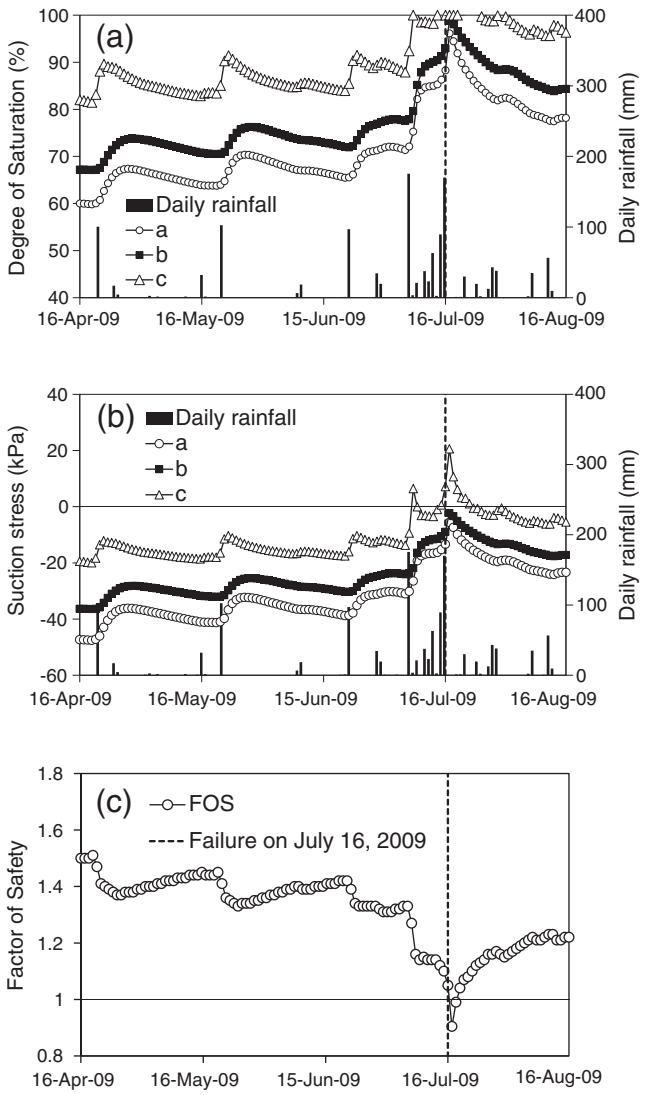

Fig. 6. Simulated results at Hadong site: (a) the effective degree of saturation vs. time, (b) suction stress vs. time, and (c) safety factor vs. time.

The results in Fig. 6a and b further illustrate the variability of soil wetness and effective stress with respect to time along the surface of failure. The 3 points *a*, *b*, and *c* are the locations shown in Fig. 2a, representing the upper, middle, and lower regions, respectively along the failure surface. As shown, the degree of saturation increases from 60% to 97% at point *a* near the top and from 67% to 100% at point *b* near the middle of the slip surface. The water table where pore water pressure is zero is just below the toe of the failure surface shown in Fig. 5a and rises to the slope surface above the toe shown in Fig. 5b. As a result, at point *c*, the degree of saturation is always higher and approaches the saturated state earlier than that at the other points on the slip surface. As shown in Fig. 6b, suction stress increases from −47 kPa to −3.4 kPa near the top point *a* and from −36 kPa to 0.6 kPa near the middle point *b* during infiltration. In particular, the region near the toe (point *c*) experiences significant wetting process in July and reaches full saturation and positive suction stress (pore water pressure) of 20.6 kPa.

The dynamics of the computed FOS during the heavy rainfall episode is shown in Fig. 6c. Initially the FOS is 1.5, but it decreases gradually until June 6 to 1.33. Rainfall of 586 mm during the 10 days prior to July 16 leads to an abrupt decrease in the FOS to 1.05 when the failure occurred on July 16 and 0.90 on July 17. As shown, the predicted FOS successfully simulates timing of the actual failure event because the limit equilibrium state or FOS = 1.0 was simulated between July 16 and 17. As a result of reduction in pore water pressure or effective stress along the slip surface (Figure 5b), the FOS reduces to a minimum of ~1.0 on July 16, 2009 when the failure occurred. The accurate reconciliation of the occurrence of the failure event indicates that the hydromechanical framework employed in this case reconnaissance is able to predict rainfall-induced instability described by changes in the FOS by a few percent.

5.2. Pohang site

The simulated distributions of pore water pressure on March 31 and June 27, 2011 are shown in Fig. 7. Fig. 7a shows the initial pore water pressure distribution before the rainy season obtained for a steady state using a monthly rainfall of 45 mm (infiltration rate of 5.6×10^{-9} m/s). At this stage (on March 31, 2011), the pore water pressures within the entire residual soil domain vary from −90 kPa to −30 kPa.

Starting on April 1, 2011 under time-varying rainfall shown in Fig. 8, the pore pressure increases to greater than −40 kPa in the residual soil layer and, to higher than −5 kPa near the slip surface, when the Pohang slope failed at the end of June. On June 27, 2011, the water table rises to the lower portion of the slope face (zero pore water pressure contour shown in Figure 7b). As shown in Fig. 7b, pore water pressure increases

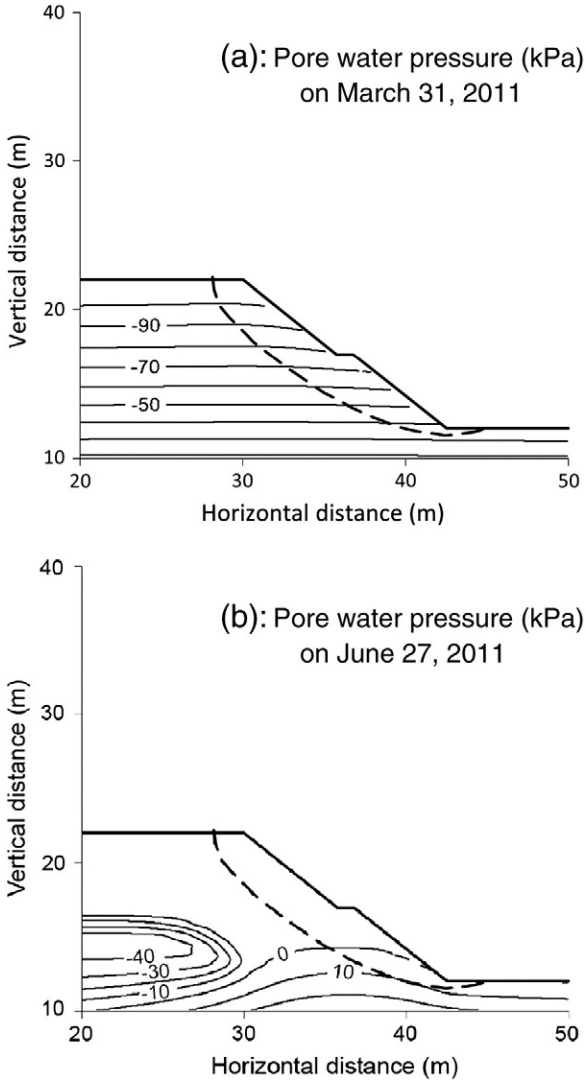

Fig. 7. Simulated results at Pohang site: (a) pore water pressure on March 31, 2011, and (b) pore water pressure on June 26, 2011.

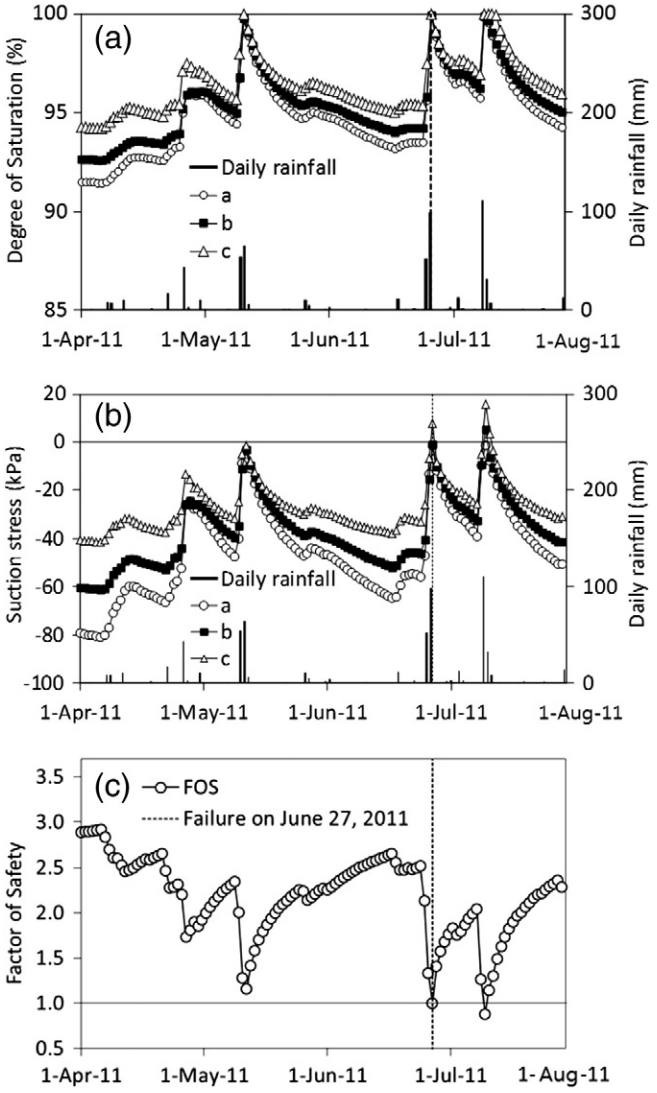

Fig. 8. Simulated results at Pohang site: (a) the effective degree of saturation vs. time, (b) suction stress vs. time, and (c) safety factor vs. time.

along the slip surface due to the three-month rainfall episode of 420 mm.

Fig. 8a shows the simulated time-series of the degree of saturation (hereafter saturation) at three representative points along the surface of failure (see Figure 2b for the locations of these points). According to the SWRC shown in Fig. 3a, the residual soil (MH soil) at Pohang site has higher degree of saturation than the soils at the other site when matric suction is less than 100 kPa or the initial saturations are greater than 90% as shown in Fig. 8a. Due to the 3-month long heavy rainfall episode, the saturation along the entire slip surface increases to nearly 100% by the end of June. As shown in Fig. 8b, suction stress fluctuates during the 3-month period, but increases from −80 kPa to −1.5 kPa at point *a* and from −41 kPa to 7.6 kPa at point *c* between April 1 and the end of June, indicating that effective stress has been reduced by 79 kPa at point *a* and by 49 kPa at point *c* during this time span.

The resulting variation in the FOS of the slope due to the variation in effective stress is shown Fig. 8c. Initially on April 1, 2011, the FOS is 2.8 and then it fluctuates but follows a decreasing trend. On May 10–11, a 2-day rainfall of 120 mm infiltrates into the slope, resulting in near saturation at all 3 points along the slip surface, as shown in Fig. 8b, and the FOS decreased abruptly to 1.16 on May 12 (Figure 8c). The FOS rebounded quickly upon the cessation of rainfall after this period. From June 25–27, another heavy rainfall event (151 mm in 2 days) occurred, leading to the FOS reaching 1.0 at the time failure occurred on June 27. The simulated FOS closely mimics the failure event at this site. The remarkably close prediction of the occurrence of the failure at this site again demonstrates that the hydromechanical framework for variably saturated slopes can predict the failure of slopes under transient seepage conditions by simulating a few percent change in the FOS defined by the LE analysis.

6. Summary and conclusions

We present two case studies of failure of engineered cut slopes due to rainfall in Korea. The traditional LE analysis with a finite element scheme is expanded to unsaturated conditions using a generalized effective stress framework. The framework involves two major enhancements to the previous LE analysis with finite element methods: (1) implementing a unified effective stress for all saturations, and (2) accounting for the change of wetness and effective stress due to transient unsaturated flow. Because effective stress is represented by the SSCC, and the SSCC and the SWRC have been recently unified by the same set of hydromechanical parameters, the expanded limit-equilibrium methodology only requires the addition of a few hydromechanical parameters. Specifically, in addition to the drained cohesion c' and friction angle ϕ' for shear strength, porosity θ_s, and

saturated hydraulic conductivity k_s, only three unsaturated hydromechanical parameters are needed to conduct slope stability under variably saturated conditions. The three unsaturated hydromechanical parameters are as follows: residual moisture content θ_r, air-entry pressure u_b, and pore-size parameter n. These three parameters, together with porosity θ_s, and saturated hydraulic conductivity k_s, are sufficient to define a material's SWRC, HCF, and SSCC.

The hydromechanical framework based on suction stress is used to reconstruct failure events of two engineered cut slopes in Korea to examine its validity, applicability, and accuracy. Using recorded rainfall data, measured shear strength and SWRC data, and site geology, transient limit equilibrium analysis implemented in a finite element framework was conducted for reconstruction of the failure events at each of the two slopes. At Hadong and Pohang sites, slope failures occurred after several days of unusually heavy rainfall and two days heavy rainfall when conditions along the entire failure surface were nearly saturated. The variation of soil wetness and effective stress could be simulated based on SWRC and SSCC, in which the degree of saturation increases and effective stress decreases along the surface of failure due to rainfall. In both cases, changes in pore water pressure or suction stress or of ~80 kPa are responsible for the failure of the slope. We find that, despite differences in slope geometry, hydromechanical properties, shear strength, and rainfall history, failure occurs under variably saturated conditions when the factor of safety approaches its minimum or 1.0. At the two sites, the framework is capable of predicting the actual failure times within a matter of days and the factor of safety within a few percent to the LE state (FOS = 1.0). Based on the case studies of the two failure events, it is concluded that the expanded hydromechanical framework can be used to accurately analyze and predict the failure of unsaturated engineered slopes under transient rainfall conditions. Traditional slope design methodology provides the worst-case scenario that employs the saturated shear strength and the conservative ground water table location near the slope surface. If engineers determine the stable slope inclination based on the effective stress principle for unsaturated soil in slope stability analysis and designs, the engineered slopes can be designed more accurately or less conservatively than the traditional methodology.

Acknowledgments

This research is partially supported by grants from Korean NRF (2012R1A1A2001001) to SO, a grant from the US NSF (CMMI-0855783) to NL, which are greatly appreciated.

References

Bishop, A.W., 1954. The Use of Pore-Pressure Coefficients in Practice. Geotechnique 148–152.
Borja, R.I., White, J.A., 2010. Continuum deformation and stability analyses of a steep hillside slope under rainfall infiltration. Acta Geotech. 5, 1–14. http://dx.doi.org/10.1007/s11440-009-0108-1.
Buscarnera, G., Whittle, A., 2012. Constitutive modelling approach for evaluating the triggering of flow slides. Can. Geotech. J. 49 (5), 499–511.
Crosta, G.B., Frattini, P., 2003. Distributed modelling of shallow landslides triggered by intense rainfall. Nat. Hazards Earth Syst. Sci. 3, 81–93.
Dawson, E.M., Roth, W.H., Drescher, A., 1999. Slope stability analysis by strength reduction. Geotechnique 49 (6), 835–840.
Duncan, J.M., 1996. State of the art: limit equilibrium and finite element analysis of slopes. J. Geotech. Geoenviron. 122 (7), 577–596.
Duncan, J.M., Wright, S.G., 2005. Soil Strength and Slope Stability. John Wiley & Sons Inc., N.J. (309 pp.).
GEO-SLOPE, 2007. Geostudio 2007. GEO-SLOPE International, Ltd., Calgary, Canada.
Godt, J.W., Baum, R., Lu, N., 2009. Can landslides occur under unsaturated soil conditions? Geophys. Res. Lett. 36, L02403. http://dx.doi.org/10.1029/2008GL035996.
Godt, J.W., Sener, B., Lu, N., 2012. Stability of infinite slope under transient infiltration conditions. Water Resour. Res. 48, W05505. http://dx.doi.org/10.1029/2011WR011408.
Griffiths, D.V., Lane, P.A., 1999. Slope stability analysis by finite elements. Geotechnique 49 (3), 387–403.
Griffiths, D.V., Lu, N., 2005. Unsaturated slope stability analysis with steady infiltration or evaporation using elasto-plastic finite elements. Int. J. Numer. Anal. Methods 29, 249–267.
Hoek, E., Bray, J., 1981. Rock Slope Engineering, 3rd edition. The Institute of Mining and Metallurgy, London (358 pp.).
Iverson, R.M., 2000. Landslide triggering by rain infiltration. Water Resour. Res. 36 (7), 1897–1910.
Krahn, J., 2003. The 2001 R.M. Hardy Lecture: the limits of limit equilibrium analyses. Can. Geotech. J. 40, 643–660.
Lee, S.-G., Hencher, S.R., 2009. The repeated failure of a cut-slope despite continuous reassessment and remedial works. Eng. Geol. 107, 16–41.
Lu, N., Godt, J.W., 2008. Infinite slope stability under unsaturated seepage conditions. Water Resour. Res. 44, W11404. http://dx.doi.org/10.1029/2008/WR006976.
Lu, N., Kaya, M., 2013. A drying cake method for measuring suction stress characteristic curve, soil–water retention, and hydraulic conductivity function. Geotech. Test. J. 36, 1–19. http://dx.doi.org/10.1520/GTJ20120097.
Lu, N., Likos, W.J., 2004. Unsaturated Soil Mechanics. Wiley, New York (564 pp.).
Lu, N., Likos, W.J., 2006. Suction stress characteristic curve for unsaturated soils. J. Geotech. Geoenviron. 132 (2), 131–142.
Lu, N., Godt, J., Wu, D.T., 2010. A closed-form equation for effective stress in unsaturated soil. Water Resour. Res. 46. http://dx.doi.org/10.1029/2009WR008646.
Lu, N., Sener, B., Wayllace, A., Godt, J.W., 2012. Analysis of rainfall-induced slope instability using a field of local factor of safety. Water Resour. Res. 48, W09524. http://dx.doi.org/10.1029/2012WR011830.
Lu, N., Wayllace, A., Oh, S., 2013. Infiltration-induced seasonally reactivated instability of a highway embankment near the Eisenhower Tunnel, Colorado, USA. Eng. Geol. 162, 22–32.
Morgenstern, N.R., Price, V.E., 1965. The analysis of the stability of general slip surface. Geotechnique 15 (4), 289–290.
Mualem, Y., 1976. A new model for predicting the hydraulic conductivity of unsaturated porous media. Water Resour. Res. 12, 593 ~ 622–593 ~ 622.
Park, Y.M., 2013. Report of safety inspection and redesign on CUT slopes in Hadong–Pyeongsari road construction works. Halla E&C Co., Seoul, Korea (in Korean).
Peterson, K.E., 1955. The early history of circular sliding surfaces. Geotechnique 5, 275–296.
Richards, L.A., 1931. Capillary conduction of liquids through porous mediums. J. Appl. Phys. 1 (5), 318–333.
Song, Y.-S., Hwang, W.K., Jung, S.-H., Kim, T.-H., 2012. A comparative study of suction stress between sand and silt under unsaturated conditions. Eng. Geol. 124, 90–97.
Spencer, E., 1967. A method of analysis of embankments assuming parallel interslice forces. Geotechnique 17 (1), 11–26.
Ugai, K., Leshchinsky, D., 1995. Three-dimensional limit equilibrium and finite element analyses: a comparison of results. Soils Found. 35, 1–7.
van Genuchten, M.T., 1980. A closed-form equation for predicting the hydraulic conductivity of unsaturated soils. Soil Sci. Soc. Am. J. 44, 892–898.
van Genuchten, M.T., Leij, F.J., Yates, S.R., 1991. The RETC code for quantifying the hydraulic functions of unsaturated soils. Rep. EPA 600/2-91/065, U.S. EPA, Ada, OK .
Vanapalli, S.K., Fredlund, D.G., Pufahl, D.E., Clifton, A.W., 1996. Model for the prediction of shear strength with respect to soil suction. Can. Geotech. J. 33, 379–392.
Vogel, T., van Genuchten, M.T., Cislerova, M., 2001. Effect of the shape of the soil hydraulic functions near saturation on variably-saturated flow predictions. Adv. Water Resour. 24, 133–144.
Wayllace, A., Lu, N., 2011. A transient water release and imbibitions method for rapidly measuring wetting and drying soil water retention and hydraulic conductivity functions. Geotech. Test. J. 35 (1), 1–15.